Two-dimensional pattern reverse Monte Carlo method for modelling the structures of nano-particles in uniaxial elongated rubbers

2007 J. Phys.: Condens. Matter 19 335217

(http://iopscience.iop.org/0953-8984/19/33/335217)

IOP PUBLISHING JOURNAL OF PHYSICS: CONDENSED MATTER

J. Phys.: Condens. Matter **19** (2007) 330017 (9pp) doi:10.1088/0953-8984/19/33/330017

Two-dimensional pattern reverse Monte Carlo method for modelling the structures of nano-particles in uniaxial elongated rubbers

K Hagita[1], T Arai[1], H Kishimoto[2], N Umesaki[3], Y Shinohara[4] and Y Amemiya[4]

[1] Department of Applied Physics, National Defense Academy, Yokosuka 239-8686, Japan
[2] SRI Research and Development Ltd, Kobe 651-0071, Japan
[3] Japan Synchrotron Radiation Research Institute (JASRI), Hyogo 651-5198, Japan
[4] Department of Advanced Materials Science, The University of Tokyo, Kashiwa 277-8561, Japan

E-mail: hagita@nda.ac.jp

Received 12 February 2007
Published 4 July 2007
Online at stacks.iop.org/JPhysCM/19/330017

Abstract

Two-dimensional pattern reverse Monte Carlo (2D pattern RMC) analysis is performed to model the structures of nano-particles in uniaxially elongated rubbers using two-dimensional patterns of structure factor of the nano-particles obtained by time-resolved two-dimensional ultra-small angle x-ray scattering. Four spot patterns are observed for a large elongation ratio and the shapes change with increasing elongation ratio. We performed the 2D pattern RMC method for the uniaxial system in order to make a model of the structures from the two-dimensional structure factors. The preliminary results of the 2D pattern RMC analysis of the two-dimensional structure factors of silica particles in a uniaxially elongated styrene–butadiene rubber are presented.

1. Introduction

Reinforcement effects on rubbers by addition of fillers such as carbon black and silica were discovered in 1904 and widely used in industrial materials such as tyres [1]. Structures of fillers play a very important role in the reinforcement, have been widely studied in order to understand the reinforcement and have improved the properties of industrial products. The diameter of the carbon black and the silica particles used as a filler is in the range of 10–100 nm. 3D-TEM tomography is a powerful tool for studying the sub-micro-scale structure of small particles, the diameter of which is a few tens of nanometres [2–4]. However, 3D-TEM tomography is not suited to study structural changes. The observation of the condensed and large scale structures of sub-micro-size particles in a deformed elastomer by small angle x-ray scattering (SAXS) and small angle neutron scattering (SANS) has attracted much interest.

Recently, Shinohara *et al* have observed the four spot patterns in uniaxially elongated rubbers filled with spherical silica particles (diameter 100 nm) by time-resolved two-dimensional ultra-small angle x-ray scattering (2D-USAXS) [5]. It is found that the four spot patterns change with increasing elongation ratio. These four spot patterns have also been observed by Oberdisse *et al* in the silica–latex system (diameter 10 nm) under uniaxial strain by SANS experiments [6, 7]. They studied the relationship between the mechanical properties and the structure of silica particles and concluded that the silica particles inside a stretched sample show non-affine displacements. They claimed the extension of the reverse Monte Carlo algorithm to two-dimensional structure factors.

In order to study the large scale (10 μm order) structure of 100 nm size silica particles, which form a network structure, the reverse Monte Carlo (RMC) method for SAXS data covering up to a few μm scale structure is a prime candidate. The reverse Monte Carlo method is a powerful tool to obtain clear interpretations of the structures in real space from observed structure factors. For dilute polymer latexes, colloids and nanoparticles, RMC for the SAXS experimental data has been performed and the shape of an agglomerate is examined [8, 9]. On the other hand, for the case that particles/atoms form a network structure, the structure factor in the small $q\sigma$ region increases with decreasing $q\sigma$, where q is the wavenumber and σ is the diameter of a particle. In order to perform RMC analysis of this system, much larger system size (number of particles/atoms) is required than for the dilute cases because a lower limit of $q\sigma$ is much smaller than that for the dilute case. Recently, one of the present authors performed the first RMC analysis to examine the large scale (network) structure of expanded fluid Hg around critical points by using the SAXS experimental data [10], where the configurations of 100 000 Hg atoms are reproduced by RMC analysis using the structure factor observed in SAXS experiments with the help of the wide angle x-ray diffraction (XRD) data in the same thermodynamic state [11, 12]. It is confirmed that RMC analysis is a powerful tool to discuss the large density fluctuations of expanded fluid Hg appearing near the critical point. Pusztai *et al* have also examined the validity of RMC modelling including the small angle region by using the artificial structure factor, which is calculated from the configuration made by a simulation for the diffusion-limited cluster aggregation (DLCA) [13]. The particles in this RMC analysis correspond to the aggregated cluster of atoms (coarse-grained atom) instead of a single atom used in the conventional RMC analysis. They clarify that the fractal dimension of the configuration of 12 500 coarse-grained atoms by RMC analysis is consistent with that of the original DLCA configuration.

In the previous study, we have developed the two-dimensional pattern reverse Monte Carlo (2D pattern RMC) method for the uniaxial system in order to make the model of structures from the two-dimensional structure factors and examined the validity for the hard sphere system [14]. In this paper, we present the preliminary results of the 2D pattern RMC analysis of the two-dimensional structure factors due to silica particles in a uniaxially elongated styrene–butadiene rubber.

In section 2, the 2D pattern RMC analysis for the uniaxial system is explained. In section 3, the 2D pattern RMC results for nano-particles in elongated rubbers are presented. A summary is given in the last section.

2. Two-dimensional pattern RMC for uniaxial system

2.1. Reverse Monte Carlo method

The reverse Monte Carlo (RMC) analysis [15–19] is widely used as a powerful tool modelling a realistic three-dimensional structure from the structure factor of the diffraction data obtained

by x-ray and neutron scattering experiments for disordered systems. In the RMC simulation, the three-dimensional configuration is repeatedly reconstructed so that the difference between observed and calculated structure factors is minimized within errors. RMC simulation starts with the initial configuration of particles. Then, the structure factor is recalculated for a trial move, which is chosen randomly and satisfies physical constraints such as excluded volume of particles, and the difference $\Delta(\chi^2)$ of the goodness-of-fit parameter χ^2 in each move is calculated by the following equation:

$$\chi^2 = \frac{\sum_q (S^{\mathrm{exp}}(q) - S^{\mathrm{calc}}(q))^2}{\sigma_{\mathrm{std}}^2}, \tag{1}$$

where $S^{\mathrm{exp}}(q)$ denotes the structure factor obtained from experiments, $S^{\mathrm{calc}}(q)$ the calculated one, and σ_{std} is the standard deviation. For $\Delta(\chi^2) \leqslant 0$, every trial move is accepted. Trial moves which worsen the fit ($\Delta(\chi^2) > 0$) are accepted with a probability of $P = \exp(-\Delta(\chi^2)/2)$. These steps are repeated until χ^2 converges well enough. The original RMC are applied only for the one-dimensional structure data such as structure factor $S(q)$ and radial distribution function $g(r)$, which are described as a function of a wavenumber q and a distance r, respectively. Therefore, the application of original RMC is designed to model isotropic structures.

We extended the reverse Monte Carlo method for anisotropic two-dimensional patterns of structure factor $S(q_x, q_y)$ instead of one-dimensional function $S(q)$. (The detail of the calculation of two-dimensional structure factor $S(q_x, q_y)$ is given in section 2.2.) The difference $\Delta(\chi^2)$ is calculated by the following equation:

$$\chi^2 = \frac{\sum_{q_x,q_y} (S^{\mathrm{exp}}(q_x, q_y) - S^{\mathrm{calc}}(q_x, q_y))^2}{\sigma_{\mathrm{std}}^2} \tag{2}$$

instead of equation (1). For the case that $S(q_x, q_y)$ converges to unity for a large $q = \sqrt{q_x^2 + q_y^2}$, the sum is taken over q_x and q_y that satisfy condition $q_x^2 + q_y^2 < q_{\mathrm{max}}^2$. 2D pattern RMC analysis needs huge requirements of computational resources. The programming source is coded using the MPI (message passing interface) on the Earth Simulator. The Earth Simulator is a distributed memory parallel computing system consisting of 640 processor nodes interconnected by a single-stage crossbar network, where one node has eight vector processors with shared memory. Our programming code is highly optimized and its parallel work ratio is 99.855%. In product runs, we used about one hundred processors without a loss due to overheads for parallel computing.

2.2. Two-dimensional structure factor

In the framework of the 2D pattern RMC for uniaxial systems, two-dimensional structure factors are calculated as follows [14]. The structure factor of a one-component system is defined as $S(\mathbf{q}) = (1/N) \sum_{j,k} \exp(\mathrm{i}\mathbf{q} \cdot (\mathbf{r}_j - \mathbf{r}_k))$, where $\mathbf{r}_i$ stands for the position of the ith particle and N is the number of particles. It can be calculated as

$$S(\mathbf{q}) = 1 + n_0 \int \mathrm{d}\mathbf{r}\, (g(\mathbf{r}) - 1) \exp(\mathrm{i}\mathbf{q} \cdot \mathbf{r}) \tag{3}$$

by using the known radial distribution function $g(\mathbf{r})$, where $n_0 = N/L^3$ denotes the average number density. For SAXS and SANS, we can approximate q_z as 0. We present the theoretical treatment for the two-dimensional structure factor of the sample elongated in the x-direction. Here, the symmetry between y- and z-directions is assumed to hold, which is supported by 2D-USAXS experiments on elongated rubber. By assuming $q_z = 0$ and y–z symmetry, we can

rewrite the three-dimensional Fourier transformation, equation (3), into the two-dimensional one as follows.

(i) Firstly, we count the number $n(x, r_\perp)$ of particles in the unit area ($\Delta X \times \Delta R_\perp$) is $(x, r_\perp)$, where $r_\perp = \sqrt{y^2 + z^2}$.

$$n(x, r_\perp) = \frac{1}{N} \sum_i \sum_j a(x - x_i + x_j, r_\perp - r_{\perp,i} + r_{\perp,j}), \tag{4}$$

where $a(X, R_\perp)$ is unity for $|X| < \Delta X/2$ and $|R_\perp| < \Delta R_\perp/2$, and zero otherwise. The pair distribution function $\bar{g}(x, r_\perp)$ in the x–$r_\perp$ plane is obtained as

$$\bar{g}(x, r_\perp) = n(x, |r_\perp|)/(4\pi n_0 |r_\perp|). \tag{5}$$

(ii) Secondly, considering the statistical weight for $r_\perp$, the reweighted pair distribution function $\hat{g}(x, r_\perp)$ is obtained as

$$\hat{g}(x, y) - 1 = \sum_z (\bar{g}(x, \sqrt{y^2 + z^2}) - 1). \tag{6}$$

(iii) The two-dimensional structure function $S(q_x, q_y)$, which corresponds to the $S(q)$ of the one-dimensional function, can be obtained by two-dimensional Fourier transformation using the reweighted pair distribution function $\hat{g}(x, y)$ estimated in the x–y plane.

$$S(q_x, q_{r_\perp}) = 1 + n_0 \int \mathrm{d}x \, \mathrm{d}r_\perp \, (\hat{g}(x, r_\perp) - 1) \mathrm{e}^{\mathrm{i}(q_x x + q_{r_\perp} r_\perp)}. \tag{7}$$

Here, we set $\hat{g}(x, r_\perp) = 1$ for $x^2 + r_\perp^2 > r_c^2$ in order to remove the effect of the shape of the area of $(q_x, q_{r_\perp})$ in the integral equation.

3. Results

In this paper, the preliminary result of 2D pattern RMC analysis, which is applied to the structure of spherical silica nano-particles in an elongated rubber, is presented. The used sample is a styrene–butadiene rubber filled with spherical silica particles with a volume fraction of 20.2%. The diameter σ of the silica particles used is a monodispersed size distribution and 282.2 nm. The two-dimensional structure factor used as an input of 2D pattern RMC analysis is calculated by using the rescaled spherical mean approximation [20–22] due to the weakly dispersed diameter of nano-particles. First, we examined the unelongated case (the elongation ratio $\epsilon = 0$) and the case of the elongation ratio $\epsilon = 1.5$, where the elongation ratio ϵ is defined by $\Delta L/L$, L is the initial length, and ΔL is the elongation length of the sample.

Here, the volume fraction for $\epsilon = 1.5$ is equal to that for $\epsilon = 0$ because the assumption of affine deformation is considered to be good for $\epsilon = 1.5$. 2D-USAXS experiments were performed in BL20XU at SPring-8. For 300 nm size silica particles, a two-dimensional structure factor in the range of $q\sigma \simeq 1.2$–7.0 can be observed. The observed patterns of scattering intensity $I^{\exp}(q_x, q_y)$ and corresponding structure factor $S^{\exp}(q_x, q_y)$ are shown in figures 1 and 2. It is noted that the relation $S^{\exp}(q_x, q_y) \simeq S^{\exp}(q_x, q_z)$ is assessed to hold by the experiments (the data are not presented here). Here, $S^{\exp}(q_x, q_y)$ is calculated by using the rescaled mean spherical approximation. The form factor $F(q_x, q_y)$ is estimated as $F(q_x, q_y) = \int \mathrm{d}\sigma \, f(\sigma) P(q, \sigma)$, where $I^{\exp}(q_x, q_y) = F(q_x, q_y) S^{\exp}(q_x, q_y)$, $f(\sigma)$ denotes the distribution probability of the particle diameter and $P(q, \sigma)$ is the form factor of a particle whose diameter is σ, and is analytically given as $P(q, \sigma) \propto ((q\sigma/2)^{-3}[\sin(q\sigma/2) - (q\sigma/2)\cos(q\sigma/2)])^2$. Here, the validity of these treatments is confirmed for the case of a dilute silica particle system and the estimated distribution $f(\sigma)$ is in agreement with that obtained from direct TEM

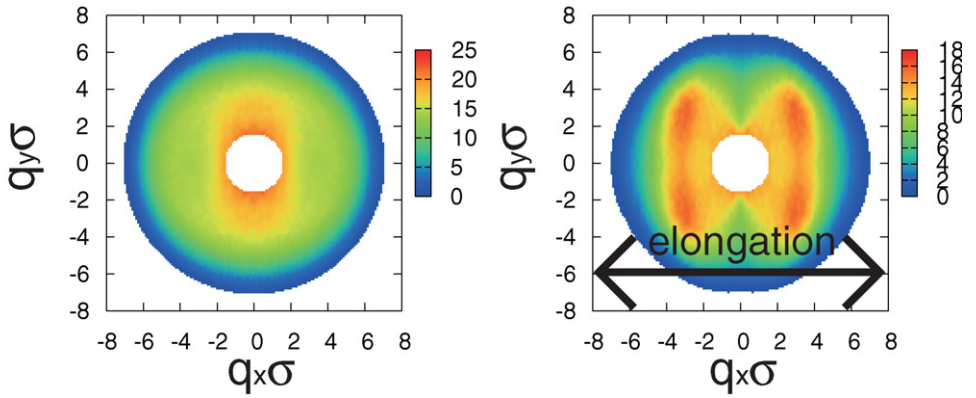

Figure 1. Scattering intensity $I^{\exp}(q_x, q_y)$: left, the unelongated case ($\epsilon = 0$), and right, the case of the elongation ratio $\epsilon = 1.5$.

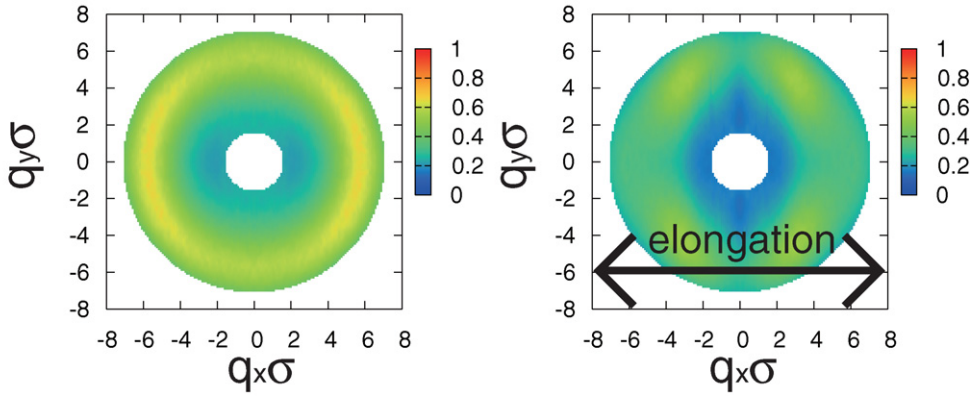

Figure 2. Structure factor $S^{\exp}(q_x, q_y)$: left, $\epsilon = 0$, and right, $\epsilon = 1.5$.

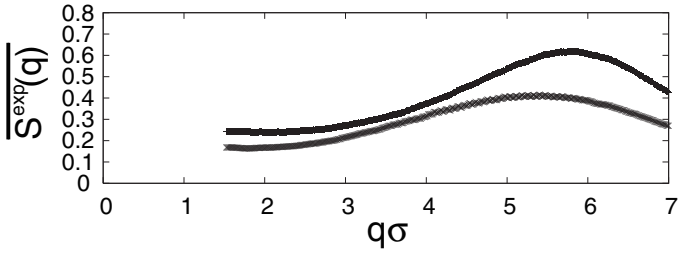

Figure 3. Azimuthally averaged structure factors: upper, $\epsilon = 0$, and lower, $\epsilon = 1.5$.

observations. Under this approximation, the factor of $S^{\exp}(q_x, q_y)$ is determined as $S^{\exp}(q_x, q_y)$ as $q\sigma \gg 1$ approaches unity, where $q = \sqrt{q_x^2 + q_y^2}$. However, this determination method of the factor seems to be wrong for RMC analysis. These features are easily observed through the azimuthally averaged structure factors $\overline{S^{\exp}(q)}$ shown in figure 3. Because the value of $\overline{S^{\exp}(q)}$ around $q\sigma \simeq 2\pi$ should be larger than unity, the appropriate scaling factor α is required for

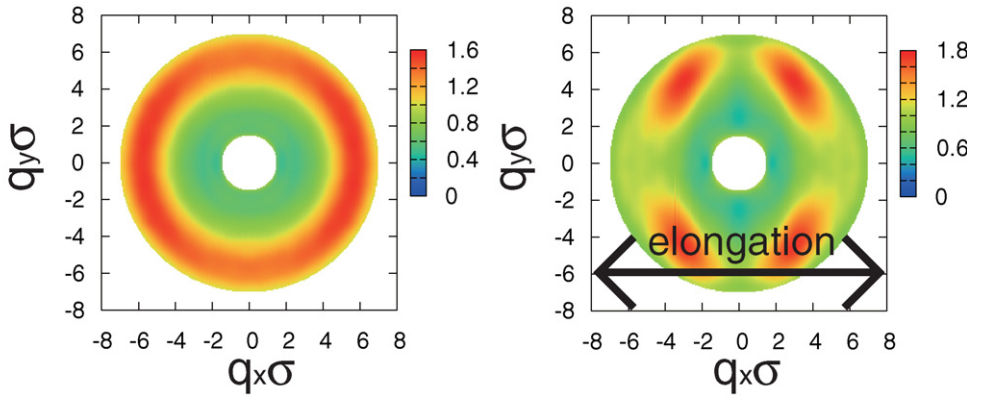

Figure 4. Structure factor $S^{\mathrm{calc}}(q_x, q_y)$ calculated from the 3D configuration obtained by 2D pattern RMC analysis: left, $\epsilon = 0$, and right, $\epsilon = 1.5$.

$S^{\mathrm{exp}}(q_x, q_y)$ in RMC analysis. Instead of equation (2), the difference $\Delta(\chi^2)$ is calculated by the following equation:

$$\chi^2 = \frac{\sum_{q_x,q_y}(S^{\mathrm{exp}}(q_x, q_y) - \alpha S^{\mathrm{calc}}(q_x, q_y))^2}{\sigma^2_{\mathrm{std}}}. \tag{8}$$

For the presented experimental data, the steepest descent method for the scaling factor α seems to be not stable. In the present analysis, the constant value of the scaling factor α is estimated from the value c, for which $\lim_{q\to\infty} \overline{S^{\mathrm{exp}}(q)} \to c$, by performing the conventional RMC program for the azimuthally averaged structure factors $\overline{S^{\mathrm{exp}}(q)}$. The values of α are estimated to be 0.4243 and 0.3094 for $\epsilon = 0$ and 1.5, respectively. The validity of these estimations of the scaling factors should be examined by the experiments. Note that the scaling factor α can be determined with the help of the wide angle x-ray scattering experiments even if the dispersion of the particle diameter is not negligibly small. For this analysis, the required range of $q\sigma$ might be wide, such as $q\sigma < 25$, in order to avoid the artifacts in $S^{\mathrm{exp}}(q_x, q_y)$ around $q\sigma \simeq 9.0$, 15.5 and 22 due to the effects of the weak dispersion of the particle diameter. Experiments in this direction are also in progress.

In the present analysis, the data in the range of $q\sigma \simeq 1.45$–7.0 are used, where the spacing of q is $\Delta q \simeq 0.06/\sigma$ and the range and the spacing of r are chosen as $r/\sigma \simeq 0$–6.9 and $\Delta r \simeq 0.03\sigma$, respectively. In order to avoid effects of the periodic boundary condition (PBC), we choose the dimension of the box of the PBC as larger than four times $(2\pi/1.45)$, and the number of particles is set to 8192. A configuration obtained from the molecular dynamics simulation of hard sphere systems is used as an initial configuration.

Figure 4 shows the two-dimensional structure factor $S^{\mathrm{calc}}(q_x, q_y)$ calculated from the obtained three-dimensional structure model of the nano-silica particles. For both cases, the behaviour of $S^{\mathrm{calc}}(q_x, q_y)$ seems to be in agreement with that of the corresponding $S^{\mathrm{exp}}(q_x, q_y)$ without the scaling factor. The slices of the snapshot are shown in figure 5.

In figure 6, bonds are drawn between particles with a distance which is smaller than 1.2 times the diameter of the silica particles, in order to clarify the shape of the large scale structure of the silica particles. Figures 7(a) and (b) show the pair distribution functions $\hat{g}(x, y)$ which present the local structure of silica particles.

In these snapshots, we can find the large density fluctuation and the large scale network structure. Such a network structure is also observed in 3D-TEM experiments [2–4], where the

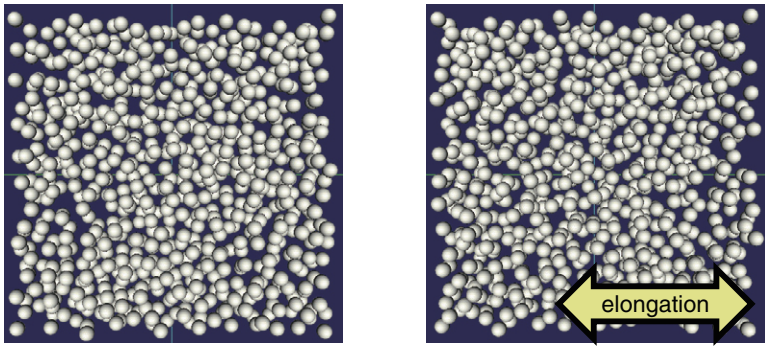

Figure 5. Slice of a snapshot: left, $\epsilon = 0$, and right, $\epsilon = 1.5$. The presented region is 6 μm $\times$ 6 μm $\times$ 1.2 μm.

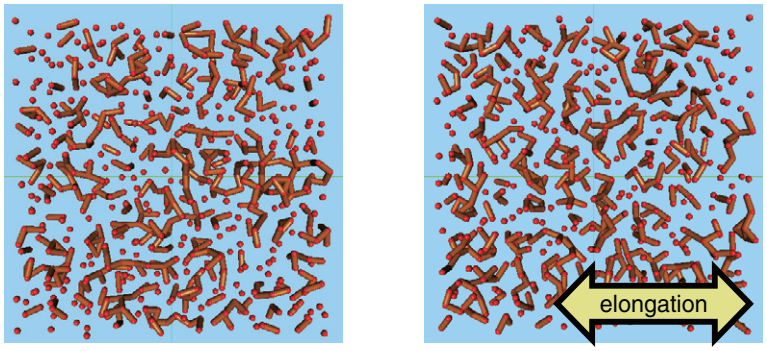

Figure 6. Slice of a snapshot with neighbouring bonds: left, $\epsilon = 0$, and right, $\epsilon = 1.5$. The same area as in figure 4 is presented.

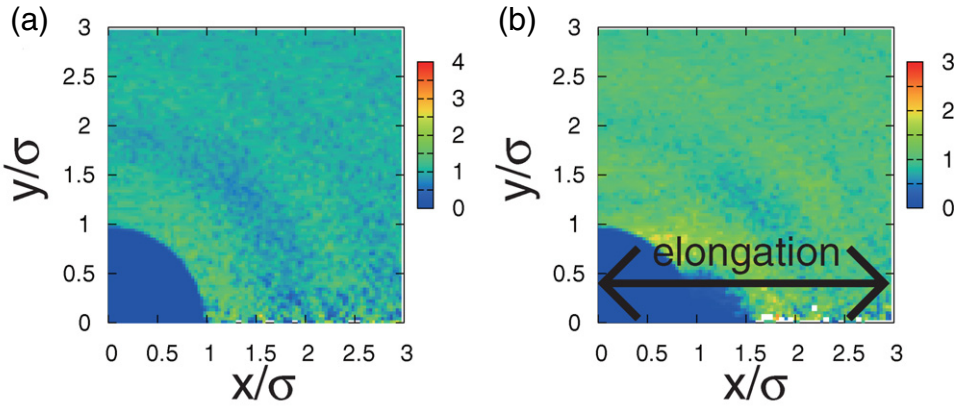

Figure 7. Pair distribution function $\hat{g}(x, y)$: (a) $\epsilon = 0$ and (b) $\epsilon = 1.5$.

diameter of nano-particles used in 3D-TEM experiments is about 20 nm and different from that used in the present 2D-USAXS experiments. Although a characteristic length of the present system cannot be estimated, we expect to be able to estimate those for the case of 100 nm size silica particles, because it is observed that the value of $S^{\exp}(q_x, q_y)$ radically increases with

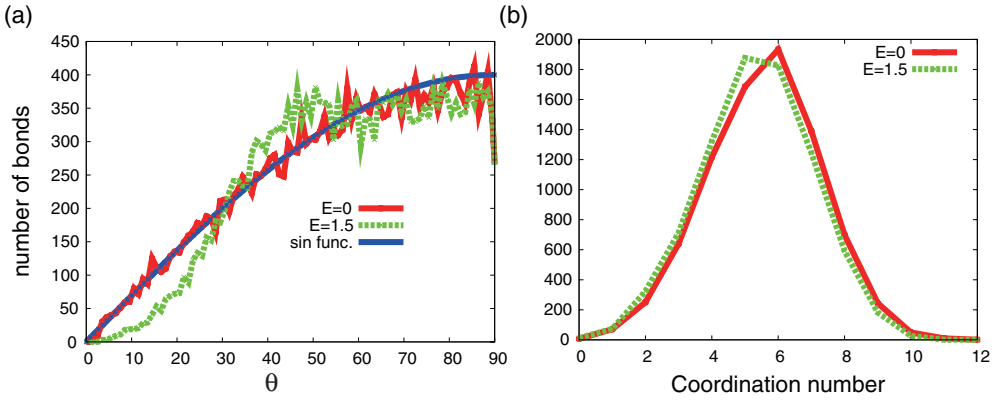

Figure 8. (a) The distribution of angles θ between the x-axis and the bonds and (b) the distribution of the coordination number.

decreasing q for small $q\sigma$. In the present case, the large value of $S^{\mathrm{calc}}(q_x, q_y)$ for $q\sigma \leqslant 1.2$ and the peak of $S^{\mathrm{calc}}(q_x, q_y)$ around $q\sigma \simeq 0.7$ is observed, although the data are not presented here. In order to clarify a characteristic length, the experimental data of small $q\sigma < 1$ are needed. In the case of 100 nm size silica particles, the structure factor for $q\sigma \simeq 0.4$–2.2 and that for $q\sigma > 2.1$ are observed by using the beam lines BL20XU and BL40B2 at SPring-8, respectively. The experiment of the 100 nm size silica particles and the 2D pattern RMC analysis using both data from BL20XU and BL40B2 is in progress.

In order to examine the difference among the different elongation ratios, the behaviour of the local structure is examined. Although the characteristic length of the density fluctuation is not reliable, we can discuss the local structure because the values of the structure factor in the corresponding q are fitted to the experimental data. Figure 7 shows the difference of the pair distribution function $\hat{g}(x, y)$ among $\epsilon = 0$ and 1.5. Although the pair distribution function $\hat{g}(x, y)$ seems to be isotropic for $\epsilon = 0$, the new peak intensity of $\hat{g}(x, y)$ increases with increasing elongation ratio. This means that the silica particles in the elongated rubber form some structure. The change of the local structure can be examined by orientations of bonds which connect two particles whose distances are not larger than 1.2 times the particle diameter as shown in figure 5. In order to examine the effect on orientations of bonds due to the elongation, figure 8(a) shows the distribution of angles θ between the x-axis (the axis of elongation) and the bonds, where this distribution for the isotropic case is proportional to $\sin\theta$. The distribution around $\theta \simeq 45°$ increases and that around $\theta \simeq 15°$ decreases with increasing elongation ratio. It is found that the change to the distribution of the number of bonds corresponds to that of $\hat{g}(x, y)$. The distribution of the coordination number is shown in figure 8(b). It is found that the distribution for $\epsilon = 1.5$ is the same as that for $\epsilon = 0$. When we compare it with $\hat{g}(x, y)$ obtained by using another initial configuration, which forms a certain regular lattice, the dependence of $\hat{g}(x, y)$ on an initial configuration is negligibly small.

4. Summary

We perform the two-dimensional pattern reverse Monte Carlo (2D pattern RMC) method for a uniaxial system and analyse the two-dimensional patterns of structure factor $S(q_x, q_y)$ for 300 nm size silica particles in the elongated rubber. The structure factor $S(q_x, q_y)$ is calculated from the scattering intensity observed in the present 2D-USAXS experiments using the rescaled

spherical mean approximation. It is found that the obtained 3D structure has a network structure, which is also observed in 3D-TEM experiments [2–4] for about 20 nm size silica particles, to examine the effect on orientations of bonds due to the elongation, the distribution of angle θ between the axis of the elongation and the bonds. It is found that the distribution around $\theta \simeq 45°$ increases and that around $\theta \simeq 15°$ decreases with increasing elongation ratio.

Acknowledgments

The present work was partially supported by the 'Program for strategic use of advanced large-scale research facilities' of the Ministry of Education, Culture, Sports, Science and Technology. We acknowledge discussions on using super-computing resources (the Earth Simulator) with Dr H Suno, Dr H Uehara, Dr H Hasegawa, Mr Y Tsuda, Mr S Shingu, Mr H Hirano and Professor K Watanabe of the Japan Agency for Marine-Earth Science and Technology. The authors thank the Japan Agency for Marine-Earth Science and Technology, Research Center for Computational Science (Okazaki National Research Facilities, National Institutes of Natural Sciences), Supercomputer Center (Institute for Solid State Physics, University of Tokyo) and Information Initiative Center (Hokkaido University) for use of the facilities. The experiments were performed at SPring-8 with the approval of JASRI (2005A0891,2006A226).

References

[1] Ferry J D 1980 *Viscoelastic Properties of Polymers* (New York: Wiley)
[2] Sugimori H, Nishi T and Jinnai H 2005 *Macromolecules* **38** 10226
[3] Ikeda Y, Katoh A, Shimanuki J and Kohjiya S 2004 *Macromol. Rapid Commun.* **25** 1186
[4] Kohjiya S, Katoh A, Suda T, Shimanuki J and Ikeda Y 2006 *Polymer* **47** 3298
[5] Shinohara Y, Kishimoto H and Amemiya Y 2005 *SPring-8 Research Frontiers 2004* p 88
[6] Oberdisse J 2006 *Soft Matter* **2** 29
[7] Rharbi Y, Joanicot M, Vacher A, Cabane B and Boue F 1999 *Europhys. Lett.* **46** 472
[8] Toth G and Pusztai L 1992 *J. Phys. Chem.* **96** 7150
[9] Toth G 2006 *J. Mol. Liq.* **129** 108
[10] Hagita K, Arai T, Inui M, Matsuda K and Tamura K 2007 *J. Appl. Cryst.* **40** S544–8
[11] Inui M, Hong X and Tamura K 2003 *Phys. Rev.* B **68** 094108
[12] Inui M, Matsuda K and Tamura K 2006 private communication
[13] Pusztai L, Dominguez H and Pizio O A 2004 *J. Colloid Interface Sci.* **277** 327
[14] Hagita K, Okamoto H, Arai T, Kishimoto H, Umesaki N, Shinohara Y and Amemiya Y 2006 *AIP Conf. Proc.* **832** 368
[15] McGreevy R L and Pusztai L 1988 *Mol. Simul.* **1** 359
[16] Keen D A and McGreevy R L 1990 *Nature* **344** 423
[17] Arai T and McGreevy R L 1998 *J. Phys.: Condens. Matter* **10** 9221
[18] McGreevy R L 2001 *J. Phys.: Condens. Matter* **13** R877
[19] Arai T and McGreevy R L 2005 *J. Phys.: Condens. Matter* **17** S23
[20] Hayter J B and Penfold J 1981 *Mol. Phys.* **42** 109
[21] Hansen J P and Hayter J B 1982 *Mol. Phys.* **6** 651
[22] Castelletto V and Hamley I W 2003 *Fibre Diffraction Rev.* **11** 36